Control Algorithms of the Longitude Motion of the Powered Paraglider

Yannick Aoustin, Martynenko Yuri

▶ To cite this version:

Yannick Aoustin, Martynenko Yuri. Control Algorithms of the Longitude Motion of the Powered Paraglider. the ASME 2012 11th Biennial Conference On Engineering Systems Design And Analysis, Jul 2012, Nantes, France. pp.1-6, 2012. <hal-00718238>

ESDA2012-82561

CONTROL ALGORITHMS OF THE LONGITUDE MOTION OF THE POWERED PARAGLIDER.

Yannick Aoustin
Institut de Recherche en Communications
et Cybernétique de Nantes,
L'UNAM, UMR CNRS 6597, CNRS,
École Centrale de Nantes, Université de Nantes,
1, rue de la Noë, BP 92101. 44321 Nantes, France
Email: Yannick.Aoustin@irccyn.ec-nantes.fr

Yuri Martynenko
Institut of Mechanics,
Moscow Lomonosov State University,
1, Michurinskii Prospect, Moscow,
119192, Russia
Email: martynenko@imec.msu.ru

ABSTRACT

The design of remotely controlled and autonomous Unmanned Aerial Vehicles (*UAVs*) is an actual direction in modern aircraft development. A promising aircraft of this type is a powered paraglider (*PPG*). In this paper, a new mathematical model is suggested for the paraglider's longitudinal motion aimed at the study of *PPG* dynamics and the synthesis of its automatic control. *PPG* under consideration is composed of a wing (canopy) and a load (gondola) with propelling unit. The *PPG* mechanical model is constructed as the system of two rigid bodies connected by an elastic joint with four degrees of freedom that executes a 2D motion in a vertical plane. The details of *PPG*'s motion characteristics including steady-states regimes and its stability have been studied. A nonlinear control law, based on the partial feedback linearization, has been designed for the thrust of *PPG*. Simulation results are analyzed. Simulation tests show that the internal dynamics are stable near the steady-state flight regime.

NOMENCLATURE

Ox_0y_0 Inertial (fixed) coordinate system.
Ax_1y_1 Moving coordinate system connected with the gondola.
$C_1x_2y_2$ Moving coordinate system connected with the canopy.
α Angle of attack [*rad*].
θ_1 Pitch angle for the gondola [*rad*].
θ_2 Pitch angle for the canopy [*rad*].
γ Climbing angle for the steady-state flight regime [*rad*].
C_1 center of mass for the gondola.
C_2 center of mass for the canopy.
A Confluence point.
A_1 Application point of the trust force.
A_2 Wheel of the gondola.
σ_1 Angle between the axis x_1 and the trust force [*rad*].
σ_2 Angle between the axis x_2 and the canopy [*rad*].
l_1 Distance between A and C_1, $d(AC_1)$ [*m*].
l_2 distance between A and C_2, $d(AC_2)$ [*m*].
l_3 Distance between A and the wheel of the gondola A_2 , $d(AA_2)$ [*m*].
l_4 Distance between A_1 and C_1, $d(A_1C_1)$ [*m*].
R Radius of the wheel of the gondola [*m*].
g Constant of gravity [$m.s^{-2}$].
ρ Density of air [kg/m^3].
ρ_1 Radius of inertia of the gondola with respect to C_1, [m^2].
ρ_2 Radius of inertia of the canopy with respect to C_2, [m^2].
m_1 Mass of the gondola [*kg*].
m_2 Mass of the canopy [*kg*].
k Stiffness coefficient for the flexible joint in A [$N{\cdot}m/radians$].
S_1 Surface of the gondola [m^2].
S_2 Surface of the canopy [m^2].
C_{D_1} Drag coefficient of the gondola.
C_{D_2} Drag coefficient of the canopy.
C_L Lift coefficient of the canopy.

C_ω Coefficient of the spin moment acting on the canopy.

T_v Trust force of the propelling unit $[N]$.

1   Introduction

Recreational flight, space recovery, rescue delivery of air cargo are privileged application fields for *PPGs* or parafoil-load-systems. From the economic viewpoint they are low cost compared to fixed wings. Their ability to glide and steer allows them to face wind-offsets, contrarily to the conventional round parachutes. They can be used for sensitive instruments or injured humans because precise and very soft landings are possible. They are lightweight and usually their size is small. In consequence their portability is an essential characteristic when they are not airborne. All these advantages enhance their appeal for use as (*UAV*).

The *PPG* is an aircraft which derives lift from a ram-air inflated canopy, under which the gondola is suspended. Their canopies are inflated by the dynamic pressure of the air flowing past them and have a cross section in the shape of an airfoil, allowing them to create lift. This capability differentiates these "parafoils" from conventional parachutes which are used to simply create drag. Thus far, the paragliders have been utilized almost exclusively for unmanned aerial vehicles (*UAV*) and sensing applications. *UAV* arouse the interest of researchers since the 60s. For example, Chambers and Boisseau [1] make a theoretical analysis to provide an understanding of some of the fundamentals of the dynamic lateral stability and control of parawing vehicles. Kuchta [2] investigates the spacecraft landing with a parachute system. Some of the earliest projects involving the usage of parafoil-based systems were discussed by Nikolaides and Knapp [3].

To determinate the analytic or interpolating expressions for aerodynamic forces acting on a paraglider in flight, it is necessary to perform a complex of experimental researches in wind tunnels, and also to solve very complicated 3D problems of computational fluid mechanics. The first preliminary wind-tunnel tests and free-flight tests for small velocities of wings in air were carried out in wind tunnel of university of Notre Dame by Nikolaides and Knapp [3]. Burk *et al.* presented an investigation of the low-speed static aerodynamic characteristics of three ram-air-inflated low-aspect-ratio parafoils in full-scale wind tunnel [4]. The aerodynamic coefficients included lift, drag and side-force coefficients; rolling, pitching and yawing moment coefficients. The experimental researches confirmed that a parafoil is similar to an airplane wing.

Parallel computational methods are described for 3D simulation of the dynamics and the fluid dynamics of a parafoil with prescribed, time-dependent shape changes by Tezduyar *et al* [5]. The mathematical model in [5] is based on the time-dependent, 3D Navier-Stokes equations governing the incompressible flow around the parafoil and Newton's law of motion governing the dynamics of the parafoil, with the aerodynamic forces acting on the parafoil calculated from the flow field.

Most parachute and payload systems are usually analyzed as one rigid body system in the same way as an airplane [6]. One of the first paper when the motion characteristics of parachute and payload system were analyzed as a two-body system is paper [7] because it has to be considered that the oscillation of the parachute is different from that of the payload.

The paper by Moulin [8] points out the importance of the modeling of the link between the parachute and the load by showing its in the dynamic behavior of this complex system. The indicated circumstance has led to occurrence of a great number of works, in which the paraglider model is designed as the system of two or several rigid bodies connected by a cylindrical (or spherical) joint. During 2D motion these systems have four degrees of freedom, for 3D motion models with eight, nine degrees of freedom or even with 15 degrees of freedom are appeared [9].

Slegers and Costello [10] study on the dynamic modelling of a parafoil with nine degrees of freedom, including three inertial positions of the joint as well as the Euler angles of the parafoil and the payload.

In [11] for an experimental vehicle ALEX a dynamic modeled is given. The physical parameters of the model are estimated and then validated using flight test data.

Hur and Valasek [12] investigated the dynamics of the BUCKEREYE vehicle considering the mechanical model with eight degrees of freedom: six for the parafoil, and two for the relative pitch and yaw attitudes of the vehicle. The parafoil and the vehicle are assumed as rigid bodies. The elasticity of the risers and suspension are ignored in modeling. In a related paper, Lund [13] details the testing of the same Buckeye powered parafoil which had been modified for use as an unmanned aerial vehicle. The aircraft was developed into a testbed for the parafoil guidance, navigation and control (*PGNC*) algorithms and sensors designed for the autonomous parafoil recovery of NASA's X-38 aircraft.

Very detailed and careful review of different models of parafoil-payload system and paraglider was carried out in paper of Yakimenko [14]. Such models are necessary for a rational choice of the basic geometrical and mass parameters of system, for readjusting nominal aerodynamic coefficients, parameters of control systems, at processing of results of flight tests and identification of mathematical models such vehicles.

Multicriteria parametrical identification of parafoil load delivery system was proposed in [15]. Based on the structural identification as an initial step toward creation of an adequate model of the parafoil, a high-fidelity model including several dozens of optimization parameters has been developed.

In [16] a control law is proposed, which includes corrections in the linear displacement, velocity, and acceleration for a powered parachute.

The paper [17] and its extended version [18] present a non-

linear dynamic model of a powered paraglider (*PPG*) and numerical simulation results obtained using the model with six degrees of freedom and two control inputs, which are the lengths of the right and left trailing edges of the parafoil canopy.

Modeling using the Lagrangian/Hamiltonian approach is also proposed in [19] and [20]. Recently, Zaitsev and Formal'skii [21] suggest a mathematical model for a planar longitudinal motion of a paraglider to synthesize its automatic control.

In contrast, in this study a new approximated dynamic model is considered for investigation *PPG* motion characteristics including steady-states regimes and its stability. A Lagrange approach is used to derive the *PPG*'s equations and aerodynamic forces are described by analytical expressions. Section 2 is devoted to the paraglider model presentation. Dynamic equations are presented, and the physical parameters of the model are chosen. In section 3 the properties of steady-state regimes of paraglider are analyzed. In section 4 the *PPG*'s control is designed which makes use of the partial feedback linearization results. We consider the amplitude of trust T_v as input and the vertical coordinate y_{C_1} of the center of mass of *PPG* as output. Proposed control provides the output tracks a desired trajectory while keeping the whole state bounded and stable. The results of numerical simulation of *PPG*'s motion are presented in section 6. Our conclusion and perspectives are offered in Section 7.

2 Mathematical model of paraglider's longitudinal motion

A schematic view of the powered paraglider is depicted in figure 1. The *PPG's* model is the system of two rigid-bodies, the gondola and the wing (canopy), connected by an elastic joint in point A. The gondola parameters have subscript 1, the canopy parameters have subscript 2. The distances between the center of mass C_1 of the gondola, the center of mass C_2 of the canopy and joint A are $AC_1 = l_1, AC_2 = l_2$. The configuration variables of the two-bodies system are

$$\mathbf{q} = (x, y, \theta_1, \theta_2)^{\mathrm{t}} \tag{1}$$

where x, y are the coordinates of joint A in the fixed coordinate system Oxy, θ_1 and θ_2 are the pitch angles for the gondola and the canopy respectively.

The positions of the center of mass C_1 of the gondola and of the center of mass C_2 of the canopy will be

$$\begin{aligned} x_{C_1} &= x + l_1 \sin\theta_1, & x_{C_2} &= x - l_2 \sin\theta_2 \\ y_{C_1} &= y - l_1 \cos\theta_1, & y_{C_2} &= y + l_2 \cos\theta_2 \end{aligned} \tag{2}$$

During the take-off roll the wheels of the gondola have con-
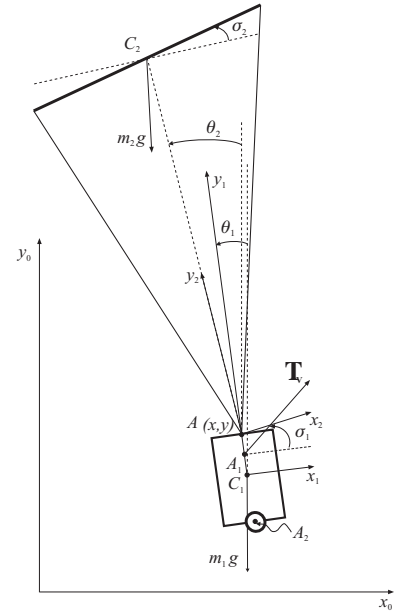
FIGURE 1. Geometric parameters and coordinate systems for the *PPG's* model (Oxy is a fixed (inertial) coordinate system, $C_1x_1y_1, Ax_2y_2$ are frames attached to the gondola and the canopy, axes y_1 and y_2 are parallel to segments C_1A and AC_2 respectively.

tact with the ground surface, so we have the unilateral constraint

$$y - l_3 \cos\theta_1 - R = 0 \tag{3}$$

The kinetic energy of *PPG* is

$$2K = \dot{\mathbf{q}}^{\mathrm{t}} \mathbf{A}(\mathbf{q})\dot{\mathbf{q}}, \tag{4}$$

where $\mathbf{A}(\mathbf{q})$ is the matrix of inertia coefficients

$$\mathbf{A}(\mathbf{q}) = \begin{pmatrix} a_{11} & 0 & a_{13}\cos\theta_1 & -a_{14}\cos\theta_2 \\ 0 & a_{11} & a_{13}\sin\theta_1 & -a_{14}\sin\theta_2 \\ a_{13}\cos\theta_1 & a_{13}\sin\theta_1 & a_{33} & 0 \\ -a_{14}\cos\theta_2 & -a_{14}\sin\theta_2 & 0 & a_{44} \end{pmatrix}$$

$$\begin{aligned} a_{11} &= m_1 + m_2, \ a_{33} = m_1(\rho_1^2 + l_1^2), \\ a_{44} &= m_2(l_2^2 + \rho_2^2), \quad a_{13} = m_1 l_1, \ a_{14} = m_2 l_2 \end{aligned}$$

The elastic and gravitational potential energies Π of the *PPG* are

$$\Pi = \frac{1}{2}k(\theta_1 - \theta_2)^2 + (a_{11}y - a_{13}\cos\theta_1 + a_{14}\cos\theta_2)g \tag{5}$$

3

where k is the stiffness coefficient of the joint linking the canopy and the gondola at the confluence point A, g is the acceleration of the free fall.

The wing (canopy) is considered as a straight-line segment centered at point C_2, the angle between axis x_2 and canopy is denoted σ_2, the unit vector $\mathbf{e}_s$ determines the direction of the canopy, see figure 2.

Due to the theorem about the simplification of the arbitrary forces system to a single resultant force and a resultant moment [22] we can replace the aerodynamic forces acting of the canopy by one resultant in the center of mass C_2 and one resultant moment $\mathbf{M}_a$, see figure 2.
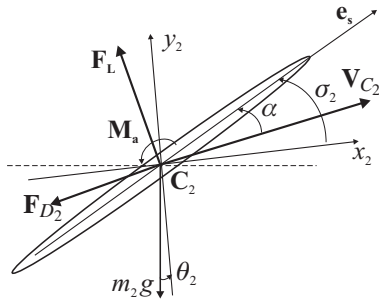
FIGURE 2. Resultant of the aerodynamic forces and spin moments applied to the canopy and attack angle.

$$|\mathbf{F}_{D_2}| = C_{D_2}\tfrac{1}{2}\rho \mathbf{V}_{C_2}^2 S_2, \quad |\mathbf{F}_L| = C_L(\alpha)\tfrac{1}{2}\rho \mathbf{V}_{C_2}^2 S_2 \qquad (6)$$

The drag force $\mathbf{F}_{D_2}$ has the opposite direction to the velocity vector of center of mass of the canopy $\mathbf{V}_{C_2}$. The direction of the lift force $\mathbf{F}_L$ is orthogonal to the velocity $\mathbf{V}_{C_2}$. In equations (6) $\tfrac{1}{2}\rho\mathbf{V}_{C_2}$ represents the dynamic pressure of the airflow, ρ is the air density, S_2 is the canopy area. The drag coefficient and the lift coefficient are denoted by C_{D_2} and C_L. The lift coefficient C_L depends on the attack angle α [23], which is the angle between the velocity of center of canopy $\mathbf{V}_{C_2}$ and the unit vector of canopy $\mathbf{e}_s$, see figure 2. We can calculate $\sin\alpha$ as function of generalized coordinates and velocities as follow

$$\sin\alpha = \frac{\sin(\theta_2 + \sigma_2)\dot{x} - \cos(\theta_2 + \sigma_2)\dot{y} - l_2\sin\sigma_2\dot{\theta}_2}{\sqrt{(\dot{x} - l_2\cos\theta_2\dot{\theta}_2)^2 + (\dot{y} - l_2\sin\theta_2\dot{\theta}_2)^2}} \qquad (7)$$

For the lift coefficient $C_L(\alpha)$ the following approximated model is used to take into account a variation of α in a large range [24]:

$$C_L(\alpha) = C_L^\alpha \sin\alpha\,\cos\alpha \qquad (8)$$

where C_L^α has a constant value. We assume the existence of a spin damping moment [25–27]:

$$M_a = -C_\omega\frac{1}{2}\rho\mathbf{V}_{C_2}S_2 l_2^2\dot{\theta}_2 \qquad (9)$$

where C_ω is a constant coefficient. This moment of aerodynamic forces tends to decrease the angular velocity of canopy $\dot{\theta}_2$ such as a viscous friction.

For the gondola we use the same model aerodynamic forces but without lifting force, $C_{L_1} = 0$. The modulus of the resultant of the drag force acting on the gondola can be written:

$$|\mathbf{F}_{D_1}| = C_{D_1}\tfrac{1}{2}\rho\mathbf{V}_{C_1}^2 S_1. \qquad (10)$$

Similarly to $\mathbf{F}_{D_2}$, the drag force $\mathbf{F}_{D_1}$ acting on the gondola has the opposite direction to the velocity of center of mass of the gondola $\mathbf{V}_{C_1}$.

Modulus T_v of the force trust that produces by a propelling unit applies to the gondola at the point A_1, $(AA_1 = l_4)$, the angle between axis x_1 of the gondola and the thrust is denoted σ_1. The points A, A_1, C_1 and A_2 are assumed to be on the same line.

Using Lagrange's equations the dynamic model of the paraglider in aerial phase can be written

$$\frac{\mathrm{d}}{\mathrm{d}t}\left(\frac{\partial K}{\partial \dot{\mathbf{q}}}\right)^{\mathrm{t}} - \left(\frac{\partial K}{\partial \mathbf{q}}\right)^{\mathrm{t}} + \left(\frac{\partial \Pi}{\partial \mathbf{q}}\right)^{\mathrm{t}} = \mathbf{Q}_a + \mathbf{Q}_t \qquad (11)$$

where $\mathbf{Q}_a$ is the generalized aerodynamic force, $\mathbf{Q}_t$ is the generalized thrust force

$$\mathbf{Q}_a = \begin{pmatrix} F_{a1x} + F_{a2x} \\[4pt] F_{a1y} + F_{a2y} \\[4pt] F_{a1x}l_1\cos\theta_1 + \\ F_{a1y}l_1\sin\theta_1 \\[4pt] -F_{a2x}l_2\cos\theta_2 - \\ F_{a2x}l_2\sin\theta_2 + M_\alpha \end{pmatrix}, \quad \mathbf{Q}_t = \begin{pmatrix} T_v\cos(\theta_1 + \sigma_1) \\[4pt] T_v\sin(\theta_1 + \sigma_1) \\[4pt] T_v l_4\cos\sigma_1 \\[4pt] 0 \end{pmatrix}$$

F_{a1x}, F_{a2x}, F_{a1y}, F_{a2y} are the projections onto fixed axes x,y the aerodynamic forces applied to the gondola and the canopy.

After computations in equation (11), we have

$$\begin{aligned}
\mathbf{A}(\mathbf{q})\ddot{\mathbf{q}} &= \mathbf{h}(\mathbf{q},\dot{\mathbf{q}}) + \mathbf{b}(\mathbf{q})T_v \\
\mathbf{h}(\mathbf{q},\dot{\mathbf{q}}) &= \mathbf{h}_c - \left(\frac{\partial \Pi}{\partial \mathbf{q}}\right)^{\mathrm{t}} + \mathbf{Q}_a \\
\mathbf{b}(\mathbf{q}) &= \big(\cos(\theta_1 + \sigma_1)\ \sin(\theta_1 + \sigma_1)\ l_4\cos\sigma_1\ 0\big)^{\mathrm{t}}
\end{aligned} \qquad (12)$$

where $\mathbf{h}(\mathbf{q}, \dot{\mathbf{q}})$ is the vector of nonlinear members, $\mathbf{h}_c$ are the vector of the Coriolis and centrifugal forces, $-\left(\frac{\partial \Pi}{\partial \mathbf{q}}\right)^{\mathrm{t}}$ are potential (gravity and elasticity) forces, $\mathbf{Q}_a$ are aerodynamic forces.

When accelerating during the launch, the paraglider moves on the ground and the vertical reaction R_y at point A_1 is

$$
\begin{aligned}
R_y = {} & a_{11}g - F_{a1y} - F_{a2y} - T_v \sin(\sigma_1 + \theta_1) + \\
& a_{13}\left(\cos\theta_1\,\dot{\theta}_1^2 + \sin\theta_1\,\ddot{\theta}_1\right) - \\
& a_{14}\left(\cos\theta_2\,\dot{\theta}_2^2 + \sin\theta_2\,\ddot{\theta}_2\right) + a_{11}\ddot{y}
\end{aligned}
\tag{13}
$$

After differentiating twice the unilateral constraint (3) we obtain the vertical component of the acceleration of point A for ground motion

$$
\ddot{y} = -l_3\left(\dot{\theta}_1^2 \cos\theta_1 + \ddot{\theta}_1 \sin\theta_1\right)
$$

When the reaction R_y given by (13) is positive adding in the right part of the first equation (12) the vector,

$$
\begin{pmatrix} 0 \\ 1 \\ l_3 \sin\theta_1 \\ 0 \end{pmatrix} R_y,
\tag{14}
$$

yields the equations of motion for the gondola rolling on the ground.

When the reaction (13) reverses its sign and becomes negative, the vehicle takes off the ground and we have to consider the equation (12). Let us remark that before to take off, the paraglider is assumed to move along the ground perfectly flat without friction.

2.1 Physical parameters of the paraglider

For the paraglider the physical parameters are:

$$
\begin{aligned}
& m_1 = 100\,kg,\ m_2 = 7\,kg,\ g = 9.81\,ms^{-2}, \\
& C_{D_1} = 0.1,\ C_{D_2} = 0.1,\ C_\omega = 0.01, \\
& l_1 = 0.48\,m,\ l_2 = 6.78\,m,\ l_3 = 0.51\,m,\ l_4 = 0.24\,m, \\
& R = 0.3\,m,\ K_j = 100\,N{\cdot}m/rad,\ \rho = 1.29\,kg/m^3, \\
& \rho_1 = 0.32\,kg/m^3,\ \rho_2 = 1.7\,kg/m^3, \\
& S_1 = 1\,m^2,\ S_2 = 30\,m^2,\ \sigma_1 = 0\,rad,\quad \sigma_2 = 0.1\,rad.
\end{aligned}
\tag{15}
$$

Let us remark that for the choice of the stiffness coefficient k of joint linking the canopy and the gondola it is possible to use the relation between the natural frequencies of *PPG* and the stiffness coefficient k. (The natural frequencies of relative motions of the gondola and the canopy can be measured during the flight [11]). For a steady-state flight of *PPG* the forces applied to paraglider (gravitational, aerodynamic, thrust) form the balanced system of forces so we can replace aerodynamic forces the vertical force $(m_1 + m_2)g$ applied to *PPG* at point C_2 and consider two-link pendulum with the fixed point C_2. If we neglect friction we can consider the conservative system. For small oscillations this system we have the following matrix equation:

$$
\mathbf{A}_0\ddot{\mathbf{q}} + \mathbf{C}_0\mathbf{q} = 0
\tag{16}
$$

where $\mathbf{A}_0$ is the constant inertia positive definite matrix and $\mathbf{C}_0$ is rigidity matrix. The linear system (16) being conservative, all the roots of its characteristic equation are on the imaginary axis. Figure 3 shows for the two non null natural frequencies dependence on the stiffness coefficient k of the joint between the canopy and the gondola
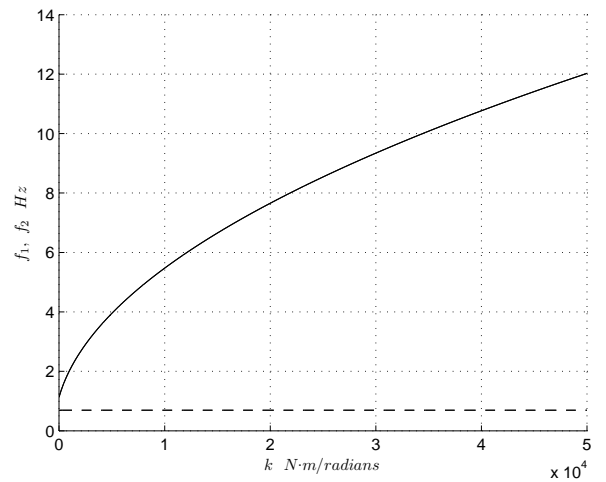

FIGURE 3. Natural frequencies as a function of the stiffness coefficient k

3 Steady-state flight regimes

If the modulus T_v of the thrust force is constant, then, using the dynamic model (12) we can find the steady-state flight regime under which there is the following steady stationary solution

$$
\begin{aligned}
& \dot{x} = V_0 \cos\gamma,\ \dot{y} = V_0 \sin\gamma, \\
& \dot{\theta}_1 = 0,\ \dot{\theta}_2 = 0,\ \theta_1 = \theta_{10},\ \theta_2 = \theta_{20},
\end{aligned}
\tag{17}
$$

where γ is the climbing angle.

In this regime, the paraglider moves uniformly along a straight line making an angle of γ with the horizontal axis Ox. Substituting particular solution (17) into differential equation (12) yields to four scalar equations relating for four unknowns: T_v, θ_{10}, θ_{20} and V_0

$$\mathbf{0} = \mathbf{h}(\mathbf{q}, \dot{\mathbf{q}}) + \mathbf{b}(\mathbf{q})T_v \qquad (18)$$

First and second scalar equations in (18) are linear equations with respect to T_v and V_0^2. After to solve these equations and the elimination of T_v and V_0^2 from third and fourth equations (18) we get two transcendental equations for the steady-state values of angles θ_{10}, θ_{20}

$$f_3(\theta_{10}, \theta_{20}, \mu) = 0, \quad f_4(\theta_{10}, \theta_{20}, \mu) = 0 \qquad (19)$$

where μ is the vector of parameters of *PPG* which include the angles γ, σ_1, σ_2, the stiffness coefficient k and other parameters.

The transcendental equations (19) define a multi-parameter set of steady-state regimes. This set can be constructed numerically with a Newton-Raphson method. If in the numerical study we use the angle γ as a single parameter, then each given (reasonable) value of γ is associated with some values of θ_{10}, θ_{20}, V_0, and T_v. These steady-state values include $\gamma = 0$ and the corresponding values of θ_{10}, θ_{20}, V_0, and T_v, with the last characteristic denoted by T_{v0}. In other words, the steady state regimes include a horizontal flight at $T_{v0} = const$. For thrust values other than T_{v0}, the paraglider in a steady-state regime follows an inclined trajectory. Therefore, the velocity of a horizontal flight cannot be changed by varying the thrust. Setting up linear equations for a small neighborhood of steady-state regimes (17), we can analyze their stability. Using the data (15) the roots of the characteristic equation of the linear model of the paraglider around the steady stationary solution (17) with $\gamma = 0.1$ are:

$$\lambda_{1,2} = -3.2370 \pm 7.0385\,i, \ \lambda_{3,4} = -0.2849 \pm 7.7878\,i, \\ \lambda_{5,6} = -0.05281 \pm 0.8164\,i. \qquad (20)$$

Steady-state regimes with highly inclined trajectories are unstable.

If for horizontal flight ($\gamma = 0$) we use the angle σ_1 as parameter in the equations (19) we can investigate the behavior of $T_{v0}(\sigma_1)$, $V_0(\sigma_1)$, $\theta_{10}(\sigma_1)$ and $\theta_{20}(\sigma_1)$, see figure 4. The thrust T_{v0} has minimum for variation σ_1 between $-0.5\ rad$ and $0.5\ rad$.

When the stiffness coefficient k increases the difference between the pitch of the gondola θ_1 and the pitch of the canopy θ_2 decreases, see figure 5.
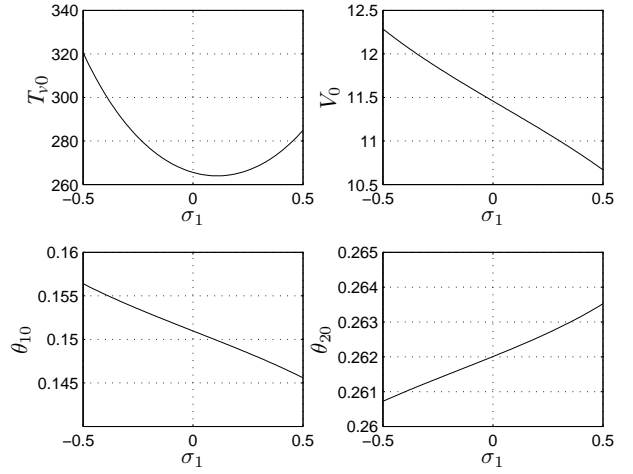
FIGURE 4. Different steady-state regimes characterized by T_{v0}, V_0, θ_{10} and θ_{20} as a function of σ_1 for the interval $-0.5\ rad < \sigma_1 < 0.5\ rad$.
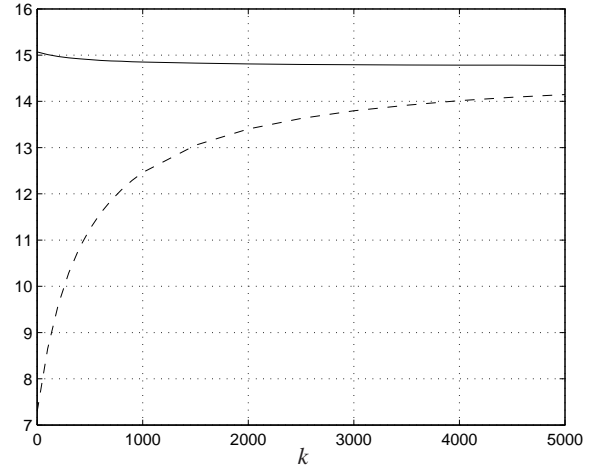
FIGURE 5. Dependence of steady state values of angles θ_{10} (solid line) and θ_{20} (dashed line) on the stiffness coefficient k.

4 Stabilization of the flight altitude

In this section we briefly inform the reader about the particular application of the routine procedure of linear control to stabilize the flight altitude. The density of air ρ depends on the altitude above the ground. However for small flight altitudes, this dependance can be considered as null. Then the motion of the paraglider does not depend on its altitude and in consequence, y is a cyclic variable. Therefore, the horizontal uncontrolled motion of the paraglider at $T_v = T_{v0} = const$ does not depend on y.

Hence this steady-state flight regime is not asymptotically stable with respect to the flight altitude. However a flight at the desired altitude can be stabilized by controlled the trust force in amplitude [21]. Zaitsev and Formal'skii proposed for the stabilizing control of a 2D paraglider without joint in the confluent point a nominal thrust amplitude T_s, closed to T_{v0}, added to a feedback with respect to the deviation of the gondola's flight altitude from the desired value and with respect to the vertical component of velocity of the point A.

$$T_v = T_s - K_p(y_{C_1} - y_{C_1}^d) - K_v \dot{y}_{C_1} \qquad (21)$$

where, $T_s = const$ is a given thrust amplitude equal or close to T_{v0}. The admissible thrust values are bounded above by a certain value T_m because the steady-state regime can become unstable, see [28]. Furthermore the thrust amplitude cannot be negative. Therefore, instead (21), we consider the feedback:

$$\overline{T_v} = \begin{cases} 0, & if \ T_v \le 0. \\ T_v, & if \ 0 \le T_v \le T_m \\ T_m, & if \ T_v \ge T_m \end{cases} \qquad (22)$$

The gains K_p and K_v, are chosen using the degree of stability $\delta > 0$ such as the eigenvalues of the matrix system of the linear model satisfy $Re\lambda_i < -\delta$ [29]. In the other cases we apply $\delta = 0$. Figure 6 shows δ, and then the asymptotical stability, obtained with the control law (22) for variations of gains K_p and K_v from 1.0 N/m to 400.0 N/m and 0.0 $N/(m.s)$ to 400.0 $N/(m.s)$ respectively.

5 Partial feedback linearization

Our objective is to make the output y_{C_1} tracks a desired trajectory $y_{C_1}^d(t)$ while keeping the whole state bounded. Time variable $y_{C_1}^d(t)$ and its time derivatives up to a sufficiently high are assumed to be known and bounded. We consider $Y = y_{C_1} - y_{C_1}^d(t) = y - l_1 cos\theta_1 - y_{C_1}^d(t)$ as output of system (12) and

$$\dot{Y} = \dot{y} + l_1 \dot{\theta}_1 sin\theta_1 - \dot{y}_{C_1}^d(t) \qquad (23)$$

defines the linearizing coordinates. The state feedback is computed when solving the following equation in T_v

$$\begin{aligned} u &= \mathbf{c}^t \ddot{\mathbf{q}} + l_1 \dot{\theta}_1^2 \cos\theta_1 - \ddot{y}_{C_1}^d(t) \\ &= \mathbf{c}^t \mathbf{A}^{-1} \mathbf{h} + l_1 \dot{\theta}_1^2 \cos\theta_1 + \mathbf{c}^t \mathbf{A}^{-1} \mathbf{b} T_v - \ddot{y}_{C_1}^d(t) \end{aligned} \qquad (24)$$
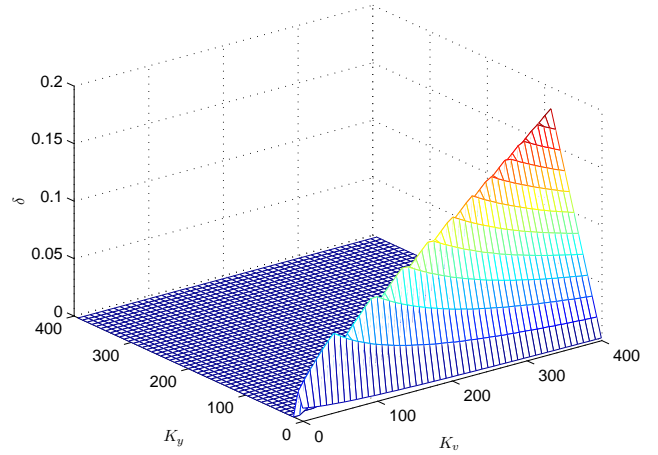
FIGURE 6. Stability degree as a function of the gains K_v and K_p obtained with the control law (22).

with $\mathbf{c}^t = \begin{pmatrix} 0 & 1 & l_1 \sin\theta_1 & 0 \end{pmatrix}^t$, which yields $\ddot{Y} = u$. We choose the control law as a simple linear double-integrator relationship between the output and the new input u

$$u = k_2 \left(\dot{y}_{C_1}^d - \dot{y}_{C_1} \right) + k_1 \left(y_{C_1}^d - y_{C_1} \right) \qquad (25)$$

where $y_{C_1}^d$ is the desired trajectory.

The trust amplitude T_v has to be chosen in the pre-feedback form

$$T_v = \frac{1}{\mathbf{c}^t \mathbf{A}^{-1} \mathbf{b}} \left(u - \mathbf{c}^t \mathbf{A}^{-1} \mathbf{h} - l_1 \dot{\theta}_1^2 \cos\theta_1 + \ddot{y}_{C_1}^d \right) \qquad (26)$$

Similarly to (22) the applied pre-feedback cannot be negative and is limited by the maximal value T_m.

The trust control (26) is defined everywhere, except at the points of singularity which are zeros of the following function

$$\mathbf{c}^t \mathbf{A}^{-1} \mathbf{b} = \frac{d(\theta_1, \theta_2)}{d_0(\theta_1, \theta_2)} \qquad (27)$$

For $m_2 \ll m_1$ it is possible to get for the function $d(\theta_1, \theta_2)$ the following asymptotic expansion

$$d(\theta_1, \theta_2) \sim \frac{\sin(\theta_1 + \sigma_1)}{m_1} \left(1 + o\left(\frac{m_2}{m_1} \right) \right)$$

The physical sense of the equality to zero the function $d(\theta_1, \theta_2)$ is the horizontal position of a vector of thrust of the *PPG* propelling unit.

To investigate the internal dynamics of *PPG* under the control law (26) with (25) we define a 4×3 dimensional matrix as follow

$$\mathbf{S(q)} = \begin{pmatrix} -\sin(\sigma_1 + \theta_1) & l_4\cos(\sigma_1 + \theta_1) & 0 \\ \cos(\sigma_1 + \theta_1) & l_4\sin(\sigma_1 + \theta_1) & 0 \\ 0 & -1 & 0 \\ 0 & 0 & 1 \end{pmatrix}$$

The three independent columns of matrix $\mathbf{S(q)}$ are in the null space of vector $\mathbf{b(q)}$, that is $\mathbf{S^t b} = 0$

Multiplying the equation (12) on the matrix $\mathbf{S^t}$ we get the zero-dynamic equation which does not content the input u

$$\mathbf{S^t}\left(\mathbf{A(q)\ddot{q}} - \mathbf{h(q,\dot{q})}\right)\big|_{y_{C_1} = y_{C_1}^d(t)} = \mathbf{0} \qquad (28)$$

The equations (28) are the system of three nonlinear ordinary differential equations of second order with the three variables x, θ_1 and θ_2. The simulation results show that near the steady-state flight regimes the solutions of internal dynamics are stable, so our control design has been solved.

For numerical simulation we choose the desired trajectory as following:

$$y_{C_1}^d(t) = \sum_{n=0}^{4} a_n \frac{(t - t_i)^n}{(t_f - t_i)^{n+1}} \qquad (29)$$

## 6 Numerical results about the tests of the partial feedback linearization

For the numerical test the chosen value of T_m to limit (26) is equal to 500 N. For the reference trajectories (29) we choose the following coefficient

$$a_0 = 0; \quad a_1 = 0; \quad a_2 = 60; \quad a_3 = -120 \quad \text{and} \quad a_4 = 60 \quad (30)$$

The chosen values for the initial and final times $t_i = 0\ s$ and $t_f = 40\ s$. Then the control law (26) is applied without discontinuities when the paraglider rolls on the ground and during the flight phase. The initial conditions are:

$$\begin{aligned} \theta_1(0) &= 0.2\ rad, a_1 = \theta_2(0) = 0.0\ rad, \\ x(0) &= 0, y(0) = 0.7998\ m \\ \\ \dot{\theta}_1(0) &= 0.2\ rad.s^{-1}, \dot{\theta}_2(0) = 0.0\ rad.s^{-1}, \\ \dot{x}(0) &= 5.0\ m.s^{-1}, \dot{y}(0) = 0\ m.s^{-1}. \end{aligned} \qquad (31)$$

Physically the initial velocity $\dot{x}(0)$ can be viewed like an initial impulsion given by the pilot. Figure 7 the profiles of the output y_{C_1} and its reference trajectory $y_{C_1}^d$ show that the choice to define a unique reference trajectory for both phases, the rolling phase and the flight phase is feasible. Just before to take off the tracking error is maximal but after the control law tracks perfectly the reference trajectory. The other generalized coordinates of the paraglider, figures 9a and 9b their time derivatives are stable during the travel.
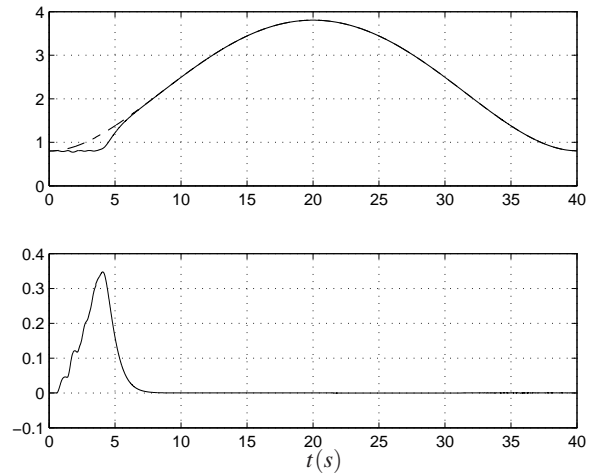

FIGURE 7. Top: Profiles of y_{C_1} (solid line) and $y_{C_1}^d$ (dashed line). Bottom: difference $y_{C_1} - y_{C_1}^d$.

Figure 10, before to take off the control law of paraglider T_v evolutes as a bang-bang control between the limit values 0 and 500 N. After for the flight phase this control law is smooth.

Figure 11, the profile of the vertical component R_y of the ground reaction confirms the activity of the control law with the presence of several oscillations. The paraglider takes off at instant $t = 3.5\ s$. The initial value of R_y is coherent with the global Paraglider's mass, (107 kg, see (15)) and tacking into account also its initial velocity.

7 Conclusion

Based on the available approach for aerodynamic forces a very soundness model of longitude motion of power paraglider are proposed. Paraglider motion has a complicated oscillatory character. The feedback linearization is very popular in robotics and gives very good results. We proposed to apply this control method to the paraglider, considering as output the center of mass of the gondola. Good preliminary results are obtained to
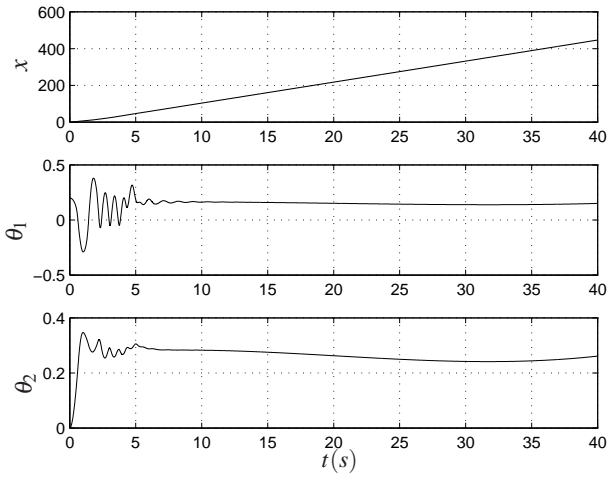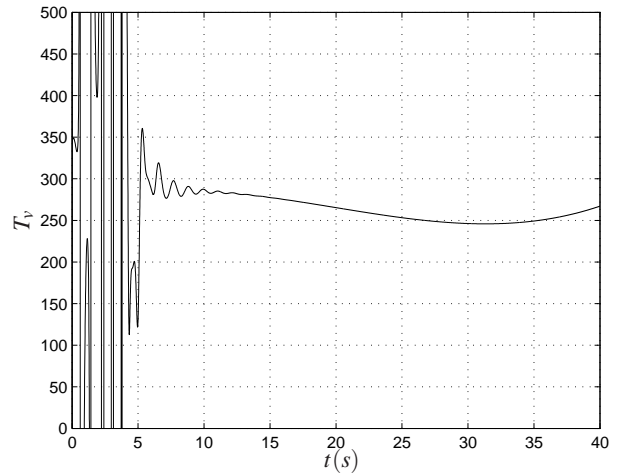
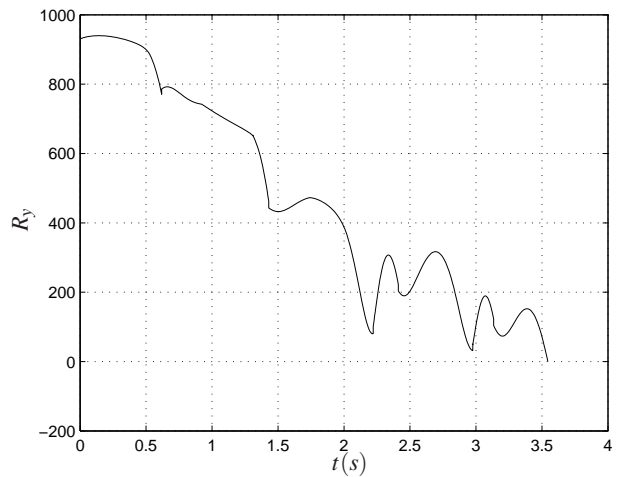**FIGURE 8**. Generalized coordinates of the Paraglider.
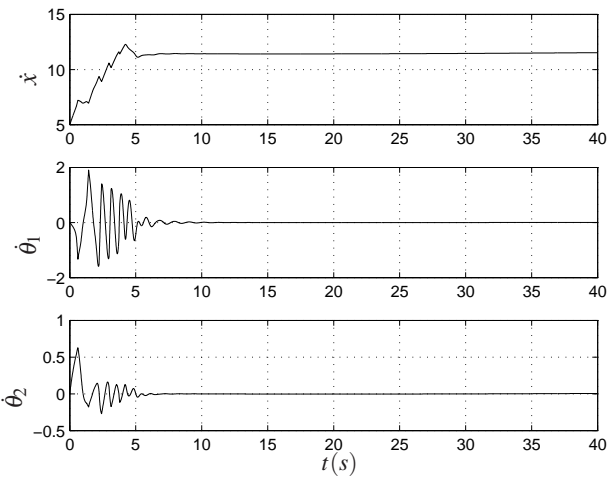
FIGURE 9. Time derivatives of the generalized coordinates of the Paraglider.

FIGURE 10. Control law T_v.

FIGURE 11. Vertical component of the ground reaction R.

prove that the feedback linearization makes sense for the control of the paraglider. However it would be interesting to explore another output with maximum feedback linearization and internal stability. See for example [30] where the computation of a suitable output function whose feedback linearization yields asymptotic stability of the full state for 2-DOF underactuated mechanical systems. However this method of feedback linearization is strongly connected to the physical system's model. It would be a drawback for the paraglider the aerodynamic forces with for example the dependance on the attack angle for the canopy, which is not so easy to estimate. In consequence it would be interesting

in future to study deeper the robustness of this control strategy to see if it is well-adapted for the so complex dynamic model of the paraglider. Furthermore an extended 3D dynamic model would useful for the design of new types of efficient powered paraglider. In future the perspectives are to consider a more exact model for the attack angle and to study the sensitivity of the control law with respect to some perturbations.

ACKNOWLEDGMENT

tional Research Scientific (CNRS) with the project PICS 3866.

REFERENCES

[1] Chambers, J. R., and Boisseau, P. C., 1966. "A theoretical analysis of the dynamic lateral stability and control of a parawing vehicle". *NASA TN D-3461*.

[2] Kuchta, B. J., 1966. "Dynamic stability of space vehicles, re-entry vehicle landing ability and control". *NASA TN CR-3461*, **12**.

[3] Nicolaides, J. D., and Knapp, C. F., 1965. "A preliminary study of the aerodynamic and flight performance of the parafoil". In AIAA Paper 1965, Proceedings of the 1st AIAA Conference on Aerodynamic Decelerator Systems, University of Minnesota, MN.

[4] Burk, S. M., and Ware, G. M., 1967. "Static aerodynamic characteristics of three rampair infalted low aspect ration fabric wings". *TND-4182, NASA*.

[5] Tezduyar, T., Kalro, V., and Garrard, W., 1997. "Parallel computational methods for 3d simulation of a parafoil with prescribed shape changes". *Parallel Computing*, **23**, pp. 1349–1363.

[6] White, F., and Wolf, D., 1968. "A theory of three- dimensional parachute dynamic stability". *Journal of Aircraft*, **5**(1), pp. 86–92.

[7] Wolf, D., 1971. "Dynamic stability of a nonrigid parachute and payload system". *Journal of Aircraft*, **8**(8), pp. 603–609.

[8] Moulin, J., 1993. "Recovery system simulation: Link modelization". In AIAA Paper 1993-1249, Proceedings of the 12th RAeS AIAA ADST Conference and Seminar, London, England.

[9] Fallon, E. J., 1991. "Parachute dynamics and and stability analysis of the queen match recovery system". In AIAA Paper 1991-0879, Proceedings of the 11th AIAA ADST Conference, Baltimore, MD.

[10] Slegers, N., and Costello, M., 2003. "Comparaison of measured and simulated motion of a controllable parafoil and payload system". *AIAA-2003-5611*.

[11] Strickert, G., 2004. "Study on the raltive motion of parafoil-load-systems". *Aerospace Science and Technology*, **8**, pp. 479–488.

[12] Hur, G. B., 2005. "Identification of powered parafoil-vehicle dynamics from modelling and flight test data". *Automatica*, **30**(7), pp. 1093–1138.

[13] Lund, D., 2004. "Unmanned powered parafoil tests for guidance, navigation, and control development". *American Institute of Aeronautics and Astronautics Inc.*, **VA 20191**.

[14] Yakimenko, O. A., 2005. "On the development of a scalable 8-dof model for generic parafoil-payload delivery system". In Proceedings of the 18th AIAA Aerodynamic Decelerator Systems Technology Conference and Seminar.

[15] Yakimenko, O. A., and Statnikov, R. B., 2005. "Multicriteria parametrical identification of the parafoil-load delivery system". In Proceedings of the 18th AIAA Aerodynamic Decelerator Systems Technology Conference and Seminar.

[16] Chambers, J. C., 2007. "Longitudinal dynamic modeling and control of powered parachute aircraft". Master thesis of science in machanical enginnering, Rochester Institute of Technology, Rochester, New York 14623.

[17] Watanable, M., and Ochi, Y., 2008. "Modeling and simulation of nonlinear dynamics of a powered paraglider". In AIAA Guidance, Navigation and Control Conference and Exhibit 18 - 21 August 2008, Honolulu, Hawaii.

[18] Ochi, Y., and Watanabe, M., 2011. "Modelling and simulation of the dynamics of a powered paraglider". *Proceedings of Institution of Mechanical Enginnering, Part G: J. of Aerospace Engineering*, **225**(4), pp. 373–386.

[19] Wise, K., 2006. "Dynamics of a uav with parafoil under powered flight flight". In AIAA Paper 2006-6795, Proceedings of AIAA Guidance Navigation and Control Conference, Keystone, Colorado, USA, pp. 1–23.

[20] Redelinghuys, C., 2007. "A flight simulation algorithm for a parafoil suspending an air vehicle". *J. of Guidance, Control Dynamics*, **30**(3), pp. 791–803.

[21] Zaitsev, P. V., and Formal'skii, A. M., 2008. "Parglider: Mathematical model and control". *Doklady Mathematics*, **77**(3), pp. 1–4.

[22] Appell, P., 1931. *Dynamique des Systèmes - Mécanique Analytique*. Paris, P. Gauthiers-Villars.

[23] Hubbard, M., and Cheng, K. B., 2007. "Optimal discus trajectories". *Journal of Biomechanics*, **40**, pp. 3650–3659.

[24] Zhukovsky, N. Y., 1891. "Soaring of birds". *Proc. of Physical Sciences Department of Nature Amateurs Society*, **4**(2), pp. 29–43.

[25] Edmondson, J. L., Sanders, E., and Claude, J., 1949. "A free-flight technique for measuring damping in roll by use of rocket-powered models and some initial results for rectangular wings". *NACA RM L9101*.

[26] Marmarkar, K. R., 1952. "Rockets". *Defence Science Journal*, **2**(4), pp. 218–221.

[27] Blyumina, K. L., and Fedyaevskii, K. K., 1966. "Loss of aerodynamic damping during rotational oscillations of isolated structural elements". *Fluid Dynamics*, **1**(5), pp. 103–105.

[28] Roitenberg, Y. N., 1992. *Automatic Control*. Nauka Moscow.

[29] Wang, G. B., Pan, B. Z., and Hou, W. Y., 2004. "Criteria for the degree of stability of the linear constant system". *Journal of Shanghai (English Edition)*, **8**(1), pp. 32–34.

[30] Maalouf, D., Moog, C. M., Aoustin, Y., and Li, S. J., 2011. "Maximum feedback linearization with internal stability of 2-dof underactuated mechanical systems". In Proceedings of the the *IFAC World Congress* 2011.